European Journal of Medicinal Chemistry 118 (2016) 340–350

Contents lists available at ScienceDirect

European Journal of Medicinal Chemistry

journal homepage: http://www.elsevier.com/locate/ejmech

Research paper

Symmetrical bis-tertiary amines as novel CXCR4 inhibitors

Renren Bai [a], Zhongxing Liang [a, b], Younghyoun Yoon [a], Shuangping Liu [c], Theresa Gaines [d], Yoonhyeun Oum [a], Qi Shi [e], Suazette Reid Mooring [d, **], Hyunsuk Shim [a, b, *]

[a] Department of Radiology and Imaging Science, Emory University School of Medicine, Atlanta, GA, 30322, USA
[b] Winship Cancer Institute, Emory University, Atlanta, GA, 30322, USA
[c] Department of Hematology and Medical Oncology, Emory University School of Medicine, Atlanta, GA, 30322, USA
[d] Department of Chemistry, Georgia State University, Atlanta, GA, 30303, USA
[e] Department of Chemistry, Emory University, Atlanta, GA, 30322, USA

ARTICLE INFO

Article history:
Received 19 February 2016
Received in revised form
14 April 2016
Accepted 15 April 2016
Available online 19 April 2016

Keywords:
Tertiary amines
CXCR4 inhibitors
Binding affinity
Matrigel invasion
Anti-inflammatory activity

ABSTRACT

CXCR4 inhibitors are promising agents for the treatment of cancer metastasis and inflammation. A series of novel tertiary amine derivatives targeting CXCR4 were designed, synthesized, and evaluated. The central benzene ring linker and side chains were modified and optimized to study the structure–activity relationship. Seven compounds displayed much more potent activity than the reference drug, AMD3100, in both the binding affinity assay and the blocking of Matrigel invasion functional assay. These compounds exhibited effective concentration ranging from 1 to 100 nM in the binding affinity assay and inhibited invasion from 65.3% to 100% compared to AMD3100 at 100 nM. Compound **IIn** showed a 50% suppressive effect against carrageenan-induced paw inflammation in a mouse model, which was as effective as the peptidic antagonist, TN14003 (48%). These data demonstrate that symmetrical bis-tertiary amines are unique CXCR4 inhibitors with high potency.

1. Introduction

C-X-C chemokine receptor type 4 (CXCR4), also known as fusin or cluster of differentiation 184 (CD184), is a seven transmembrane G-protein coupled receptor (GPCR) belonging to the Class I GPCR or rhodopsin-like GPCR family [1,2]. Stromal-derived-factor-1 (SDF-1) or C-X-C chemokine ligand 12 (CXCL12) is the major ligand of CXCR4 and the interaction recognition between CXCL12 and CXCR4 recruits cells to the organ sites with high levels of CXCL12 expression [3,4]. The CXCL12/CXCR4 axis has been shown to be involved in a number of pathological conditions, including cancer and inflammation [5,6]. CXCR4 plays a key role as a homing receptor to the lymph nodes, lung, liver, and bone. Homing, the mechanism that allows foreign tissue-origin cells to reside and proliferate, is believed to be the rate-limiting step of the multi-step metastatic process [7,8]. These suggest that the interaction between CXCL12 and CXCR4 plays a key role in the chemotaxis and homing of metastatic cells [9]. CXCR4 is overexpressed in more than 23 human cancer types [10,11], such as breast [12–14], leukemia [9], lung [15], and prostate cancers [16].

Inflammation is inextricably associated with primary tumor progression and contributes to metastatic outgrowth in distant organs [17]. The COX pathway has long been used as the major target for anti-inflammatory drugs [18]. Both traditional non-steroidal anti-inflammatory drugs (NSAIDs) and selective COX-2 inhibitors exhibit their anti-inflammatory activity by inhibiting COX-2 [18]. Nevertheless, the prolonged use of traditional anti-inflammatory drugs is associated with potential serious side effects such as kidney failure, ulcers and prolonged bleeding after an injury or surgery [19–21]. Furthermore, rofecoxib and valdecoxib were withdrawn from the market due to an increased risk of cardiovascular complications [22,23].

Accumulating evidence suggests the involvement of CXCR4–CXCL12 interaction in various inflammatory diseases, including rheumatoid arthritis, autoimmune diseases, ischemic injuries, inflammatory bowel disease, and pneumonia [24,25].

* Corresponding author. Department of Radiology and Imaging Science, Emory University School of Medicine, 1365C Clifton Road, NE, C5008, Atlanta, GA, 30322, USA.
** Corresponding author. Department of Chemistry, Georgia State University, 519A Science Annex, Atlanta, GA, 30302-4098, USA.
E-mail addresses: smooring@gsu.edu (S.R. Mooring), hshim@emory.edu (H. Shim).

http://dx.doi.org/10.1016/j.ejmech.2016.04.040
0223-5234/

Based on these findings, development of inhibitors blocking CXCR4 presents a new avenue for complementary therapeutic strategy in inflammatory diseases as well as cancer metastasis.

The first CXCR4 inhibitor to enter clinical trials for treatment of HIV infection is AMD3100 [25]. The development of AMD3100 has followed a meandering course, starting with JM1657, an impurity in commercial cyclam preparation with anti-HIV activity, and finally leading to AMD3100 [26]. Because of the preorganisation and the flexibility of the AMD3100 macrocyclic cyclam, it can bind to metal ions and form highly stable metal complexes [3]. These chelating properties are likely related to the cardiotoxicity reported in its clinical trial against HIV [26–29]. In 2008, AMD3100 was approved by FDA for stem cell mobilization [25]. Although it benefits patients with certain diseases, long term treatment can introduce lung and liver fibrosis [27]. Hence there is an urgent need to develop safe CXCR4 inhibitors that can be used in long-term treatment.

Taking AMD3100 as the lead compound, we simplified and optimized its bicyclam rings, leading to the design and synthesis of a series of novel and potent CXCR4 inhibitors [30,31]. Previously, we reported a novel small molecule, compound **2** (Fig. 1), which is now under clinical trial (Phase **II**). Compound **2** is a partial CXCR4 inhibitor with properties quite unlike that of any other reported CXCR4 antagonists. Compound **2** does not have stem cell mobilizing capability nor calcium flux modulating activity, which can be safer for long-term blockade of metastasis than other reported CXCR4 antagonists [27].

Most of our reported CXCR4 inhibitors are secondary amines. Here we attempted to design and synthesize a new series of tertiary amine compounds to explore whether these new structures will maintain the CXCR4 inhibitory effect. Meanwhile, an extensive structure-activity profile indicates that the central benzene ring is critical for high CXCR4 affinity [31]. Since pyridine derivatives have been explored for their potential as pharmaceutical agents [32], we also substituted the middle benzene ring with a pyridine framework. The structural formula was shown in Fig. 1.

2. Results and discussion

2.1. Chemistry

The synthetic route chosen to synthesize the title compounds was outlined in Scheme 1. The previous method to efficiently prepare symmetrical bis-secondary amine compounds was reductive amination of 1,4-benzenedialdehyde with phenylamine derivatives [30–32]. Since the reagents used in this preparation are secondary amines like *N*-alkyl anilines or cyclic amines, the yield is no longer satisfying. Herein, 1,4-bis(bromomethyl) benzene was used as the starting material, which reacted with corresponding secondary amines in anhydrous acetonitrile in the presence of potassium carbonate, and afforded the target compounds **Ia-p** [33]. Similarly, 2,6-bis(chloromethyl)pyridine reacted with amine derivatives in acetonitrile provided the title compounds **IIa-p**. Considering benzyl chloride is less active than benzyl bromide, cesium carbonate was used to shorten the reaction time.

2.2. Primary binding affinity screening

All the compounds were initially screened with a binding affinity assay as described in our previous publications [31,34]. This assay involves competition of a potent CXCR4 peptidic inhibitor, TN14003, with the target compounds **Ia-p** and **IIa-p**. MDA-MB-231 cells were pre-incubated with compounds at concentrations of 1, 10, 100, and 1000 nM, then incubated with biotinylated TN14003 and streptavidin-conjugated rhodamine to determine the binding efficiency of the new compounds to the CXCL12 binding domain of CXCR4. The effective concentration (EC) is defined as the lowest concentration at which a significant reduction in the rhodamine fluorescent color is observed as compared to the control reflecting the competitive displacement by peptide TN14003. Thus, this screening is a semi-quantitative, first pass measure of the level of activity.

Just like the reported secondary amine derivatives, the symmetrical bis-tertiary amine framework also successfully retained the significant CXCR4 antagonistic effect. Nineteen of the 32 synthesized compounds exhibited moderate to good activity (≤1000 nM) in blocking the binding of peptide TN14003 to CXCR4 (Table 1 and Fig. 2). Ten substances displayed potent binding affinity, with EC values from 1 to 100 nM. They were all comparatively more effective than the reference drug, AMD3100 (1000 nM).

When only the benzene central ring was substituted with a pyridine ring and the structure of side chains remained the same, most of the compounds demonstrated better activity. This result indicates that the central pyridine linker is well tolerated and further modification of the middle ring functionality is a reasonable strategy.

Surprisingly, if the terminal rings of the side chains were non-aromatic instead of aromatic amines (for example, a pyrrolidine, piperidine, or morpholine ring), the target compounds showed improved binding affinity to the compounds possessing aromatic side chains. Compounds **IIa** and **IIb** showed an EC of 1 nM, and experienced 1000-fold improvement compared with AMD3100. In addition, the substituent group introduced onto the 3′ position of the terminal ring may enhance the binding effect. By contrast, most compounds substituted into the 2′ or 4′ positions are less active or even inactive. For example, **Ik**, **IIk** and **IIg** all showed an EC of 10 nM, while compounds **If**, **Ih**, **Ij**, **IIf**, and **IIk** were not effective even at 1000 nM.

2.3. Matrigel invasion assay

To model *in vitro* metastasis, a Matrigel invasion assay was used as the functional assay [31,34]. This assay was performed for those compounds with an EC value lower than 1000 nM in the binding affinity assay to test whether they could block the CXCR4/CXCL12-mediated chemotaxis and invasion at a single concentration of 100 nM. The compounds and cells were added to the upper chamber and CXCL12 was added to the lower chamber as a chemoattractant. A layer of Matrigel matrix-coated permeable support (8 μm pore diameter) separates the upper and lower chambers. If the compounds demonstrate a strong CXCR4 inhibitory effect, fewer cells are able to move through the Matrigel. The results of

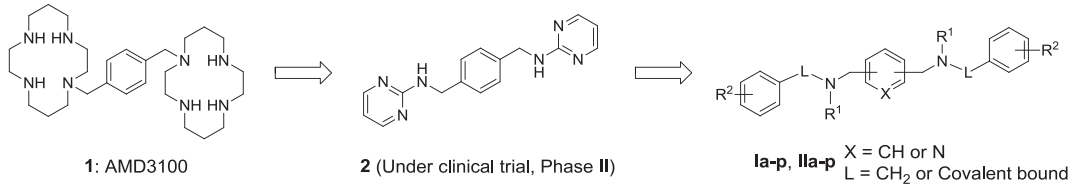

Fig. 1. Strategy for the design and optimization of anti-CXCR4 compounds.

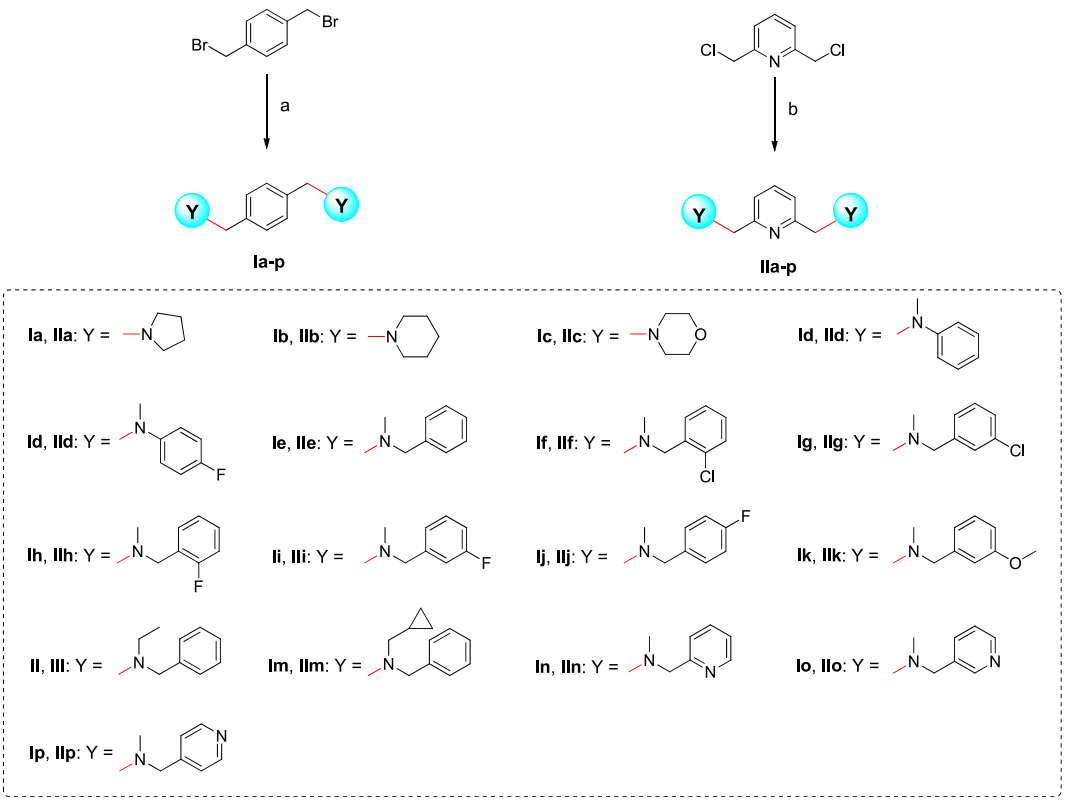

Scheme 1. Reagents and conditions to make our compounds: (a) CH_3CN, K_2CO_3, reflux, 3 h, 78–95%; (b) CH_3CN, Cs_2CO_3, reflux, 5 h, 70–90%.

Table 1
Preliminary effective concentration (EC) of anti-CXCR4 compounds in our binding affinity assay.

Compd	EC (nM)	Compd	EC (nM)	Compd	EC (nM)	Compd	EC (nM)
Ia	1000	**Ii**	>1000	**IIa**	1	**IIi**	>1000
Ib	10	**Ij**	>1000	**IIb**	1	**IIj**	1000
Ic	>1000	**Ik**	10	**IIc**	100	**IIk**	10
Id	1000	**Il**	1000	**IId**	1000	**III**	>1000
Ie	100	**Im**	1000	**IIe**	1000	**IIm**	1
If	>1000	**In**	>1000	**IIf**	>1000	**IIn**	10
Ig	1000	**Io**	>1000	**IIg**	10	**IIo**	>1000
Ih	>1000	**Ip**	>1000	**IIh**	1000	**IIp**	>1000
AMD3100	1000						

Matrigel invasion were summarized in Fig. 3 and Fig. 4.

The invasion evaluation proved that most of the selected compounds performed well in both the binding affinity assay and blocking of Matrigel invasion assay. Only **Ib**, **Ik** and **IIe** exhibited an inhibitory rate below 50%. The potency of **Ie** (66.4%), **IIb** (65.3%), **IIc** (68.9%), **IIg** (88.6%), **IIk** (76.7%), **IIm** (100%) and **IIn** (72.6%) was superior to the reference drug AMD3100 (62.0%).

2.4. *In vivo* suppression against carrageenan-induced paw edema

CXCR4 plays a key role in the recruitment of inflammatory cells to sites of inflammation. Blocking CXCR4 is a therapeutic strategy in inflammatory diseases [24]. Previously, we reported utilizing a carrageenan-induced mouse paw edema model as an efficient model to evaluate the *in vivo* CXCR4 antagonistic activity for CXCR4 inhibitors [27,31]. It is a widely used test to assess anti-inflammatory activity *in vivo*. On the basis of the *in vitro* assay results, four of the best compounds (**IIg**, **IIk**, **IIm** and **IIn**) were investigated. Because of the *in vivo* toxicity of AMD3100, we have been using TN14003 as the reference drug for our animal experiments [27,35]. As illustrated in Fig. 5, although substances **IIg** and **IIm** demonstrated excellent CXCR4 antagonistic activity, they showed very weak *in vivo* potency (<20%), which may be attributed to their metabolism or poor pharmacokinetic profile. Compound **IIk** exhibited moderate inhibition (31.0%). **IIn** showed a 50% inhibitory effect on inflammation, which was comparable to TN14003 (48%). Compared with the low success rate and high cost of the development of peptide drugs [36], small molecule CXCR4 inhibitors have practical advantages. After being treated with **IIn**, the inflammation induced in the left paw was clearly suppressed (Fig. 6). As shown in histological analysis in Fig. 7, the normal mouse paw tissue exhibits a dermis tightly connected to the epidermis through a basement membrane, and the papillary region is composed of loose areolar connective tissue (A1-3). However, the carrageenan-induced inflammatory tissue showed intense dermal papillae edema, and a dense infiltration of inflammatory cells (B1-3). Compound **IIn** significantly attenuated the mouse paw inflammation and damage in histological assay. Both the edema volume and the number of inflammatory cells decreased observably (C1-3). These data confirm that this selected anti-CXCR4 candidate can inhibit inflammation as anticipated.

Since compound **IIn**, which possesses a pyridine pharmacophore, had the best suppression effect *in vivo*, we modified the terminal ring and synthesized compounds **Io**, **Ip**, **IIo** and **IIp,** bearing a nitrogen atom at the 3′ or 4′ position. Unfortunately, these compounds exhibited poor ECs in the binding affinity assay (>1000 nM). Hence we stopped the further investigation of these compounds.

2.5. Discussion of paw edema results

Carrageenan-induced paw edema animal model is one of the

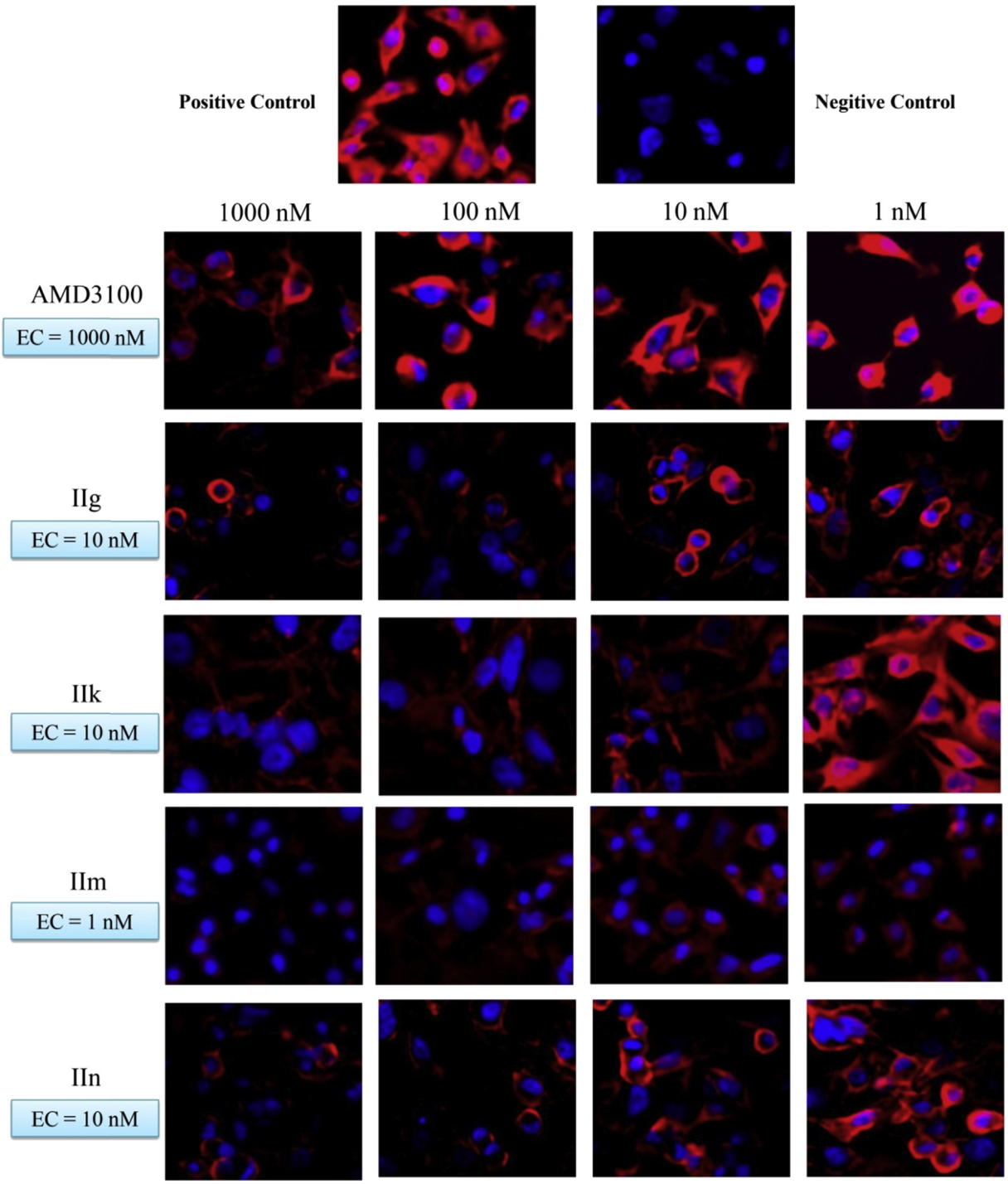

Fig. 2. Fluorescence micrographs of binding affinity assay results of four selected compounds compared to AMD3100. The effective concentration (EC) of AMD3100 is 1000 nM, while those of the compounds **IIg**, **IIk**, **IIm** and **IIn** are better, EC of 10, 10, 1, and 10 nM, respectively.

most popular *in vivo* tests to screen anti-inflammatory properties of potential drugs. Complex sequential pathways for the inflammatory response to inter dermal injection of carrageenan were described by Vinergar R. et al. [37]. Briefly, it consisted of a non-phagocytic inflammatory response followed by a phagocytic inflammatory response. The dermal nonphagocytic inflammatory response comprised edema, hyperemia, and hyperalgesia followed by hypoalgesia. The hyperalgesia and part of the edema were sensitive to cyclooxygenase (COX) inhibitors. The dermal phagocytic inflammatory response consisted of mobilization of neutrophils, monocytes, fibroblasts, and endothelial cells. While COX inhibitors reduce edema formation and hyperalgesia by blocking arachidonic acid metabolism, CXCR4 inhibitors reduce carrageenan-induced paw edema by blocking the recruitment of various inflammatory cells that are CXCR4-positive. In addition, CXCR4 has been shown to modulate NFκB that is the master switch of inflammation response [38].

Developing anti-CXCR4 drugs for inflammation indication provides an exciting avenue to target different pathways from COX which has been the major, if not the only one, target of anti-

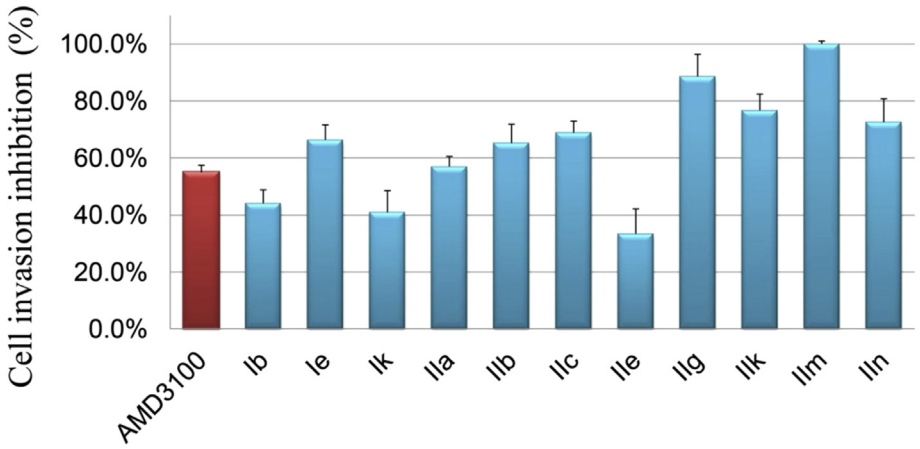

Fig. 3. Matrigel invasion inhibition of AMD3100 and anti-CXCR4 compounds.

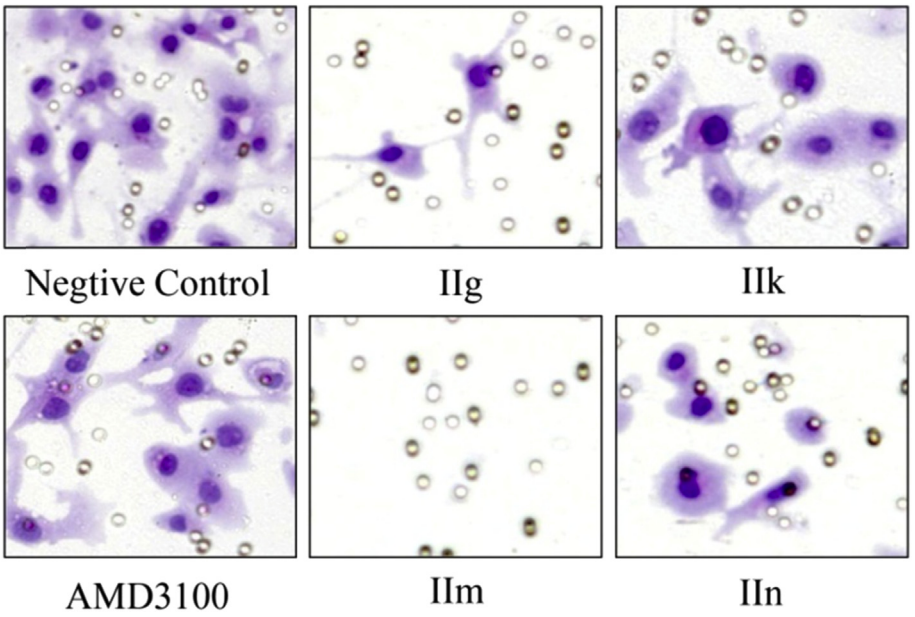

Fig. 4. Anti-Matrigel invasion effect of AMD3100 and four selected compounds. Fewer MDA-MB-231 cells are able to invade through the Matrigel after treatment with compounds **IIg**, **IIk**, **IIm** and **IIn** than AMD3100.

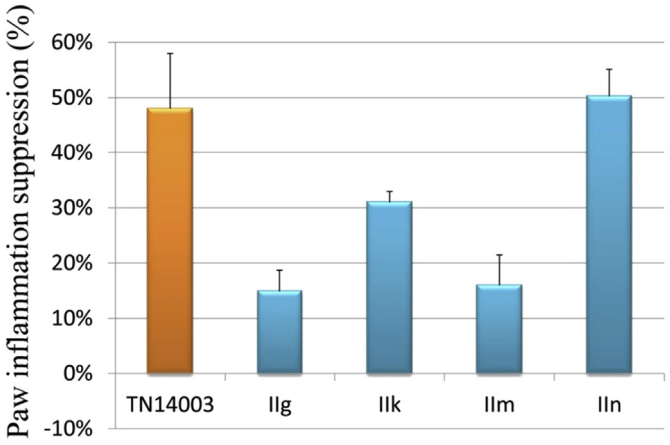

Fig. 5. *In vivo* anti-inflammatory activity of compounds **IIg**, **IIk**, **IIm** and **IIn**.

inflammation drugs. By combining drugs targeting different pathways, the efficacy will be enhanced without increasing dosage of a drug which is associated with unwanted side effects.

Previous reports on drug testing against inflammation using carrageenan-induced paw edema model were geared toward prevention by treating animals 30 min before carrageenan injection, which is clinically irrelevant [18,39]. Patients present to hospital after the fact. In our evaluation, the compounds were treated after carrageenan injected.

2.6. Molecular modeling (docking) studies

To better understanding the possible interaction between **IIn** and CXCR4, Schrodinger Maestro Package was performed based on the available crystal structure of CXCR4 (PDB code: 3ODU [40]). Fig. 8 illustrated the binding pose with the best docking score. A hydrogen bond is formed between Asp97 and one of the nitrogen atoms of **IIn**. One pyridine ring shows a π–π stacking with both His113 and Trp94. The other pyridine ring demonstrates a partially

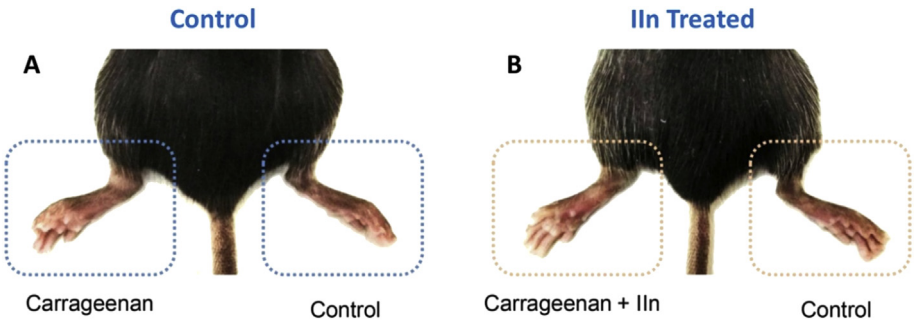

Fig. 6. Suppression effect of anti-CXCR4 compound **IIn** on carrageenan-induced mouse paw inflammation. (A) Control mouse with left paw induced inflammation by carrageenan. (B) **IIn** treated mouse with left paw induced inflammation by carrageenan with about 50% suppression.

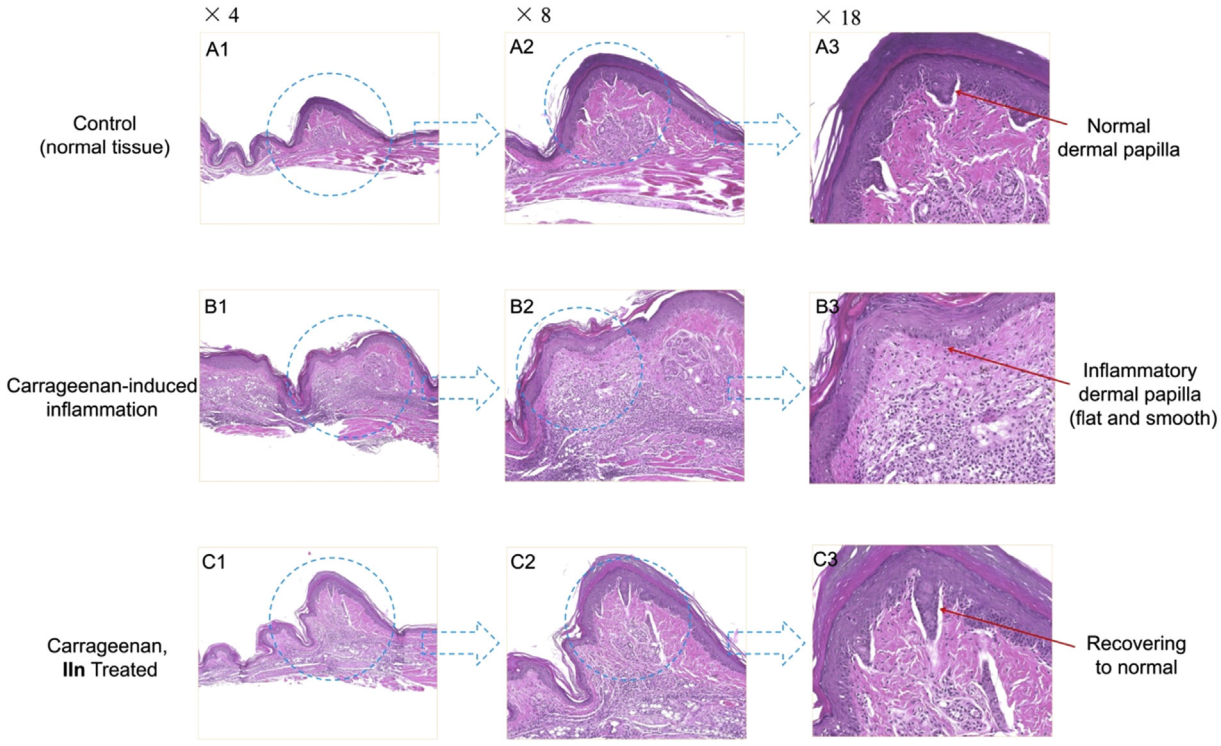

Fig. 7. Compound IIn significantly attenuated the mouse paw inflammation and damage in histological assay. Paw tissue sections were stained with H&E. The whole tissue slices were scanned/digitized by NanoZoomer 2.0 HT. Software NDP. view 2 was used to zoom in. Compared to the normal tissue (A1-3), carrageenan-induced skin inflammation exhibited intense dermal papillae edema, and a dense infiltration of inflammatory cells (B1-3). After being treated with IIn, both the edema volume and the number of inflammatory cells (dark purple) decreased observably (C1-3). (For interpretation of the references to colour in this figure caption, the reader is referred to the web version of this article.)

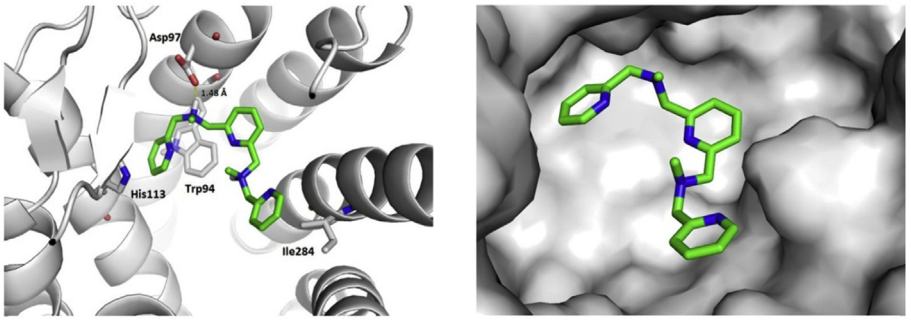

Fig. 8. A low energy predicted binding pose for compound **IIn** in the CXCR4 X-ray structure (grey). The best docking pose is illustrated by two different visualizations: ribbon (left) and protein surface (right) representations.

hydrophobic interaction with Ile284. These favorable interactions are likely contributing to the binding of **IIn** with CXCR4.

3. Conclusion

On the basis of the promising previously prepared CXCR4 inhibitor **2**, a series of novel symmetrical bis-tertiary amines, non-peptidic anti-CXCR4 small molecules, were designed and synthesized. The central benzene ring linker and side chains were modified and optimized to study the structure–activity relationship. This symmetrical bis-tertiary amine framework successfully maintained the significant CXCR4 antagonistic effect. Ten substances displayed potent binding affinity, with EC values from 1 to 100 nm. They were all comparatively more effective than the reference drug, AMD3100 (1000 nM). Most of the compounds with an EC lower than 1000 nM performed well in the invasion assay. Compounds **Ie**, **IIb**, **IIc**, **IIg**, **IIk**, **IIm** and **IIn** significantly blocked the tumor cell invasion. The inhibitory rates ranged from 65.3% to 100%, which were superior to AMD3100 (62.0%). Compound **IIn** showed a 50.3% suppressive effect against an inflammation animal model, comparable to the positive control, TN14003 (48.0%). These promising results demonstrate that symmetrical bis-tertiary amines are unique CXCR4 inhibitors with high potency.

4. Experimental section

4.1. Chemistry

4.1.1. General information

Proton and carbon NMR spectra were recorded on INOVA-400 (400 MHz) or VNMR-400 spectrometers at Emory NMR Research Center. The spectra obtained in deuteriochloroform ($CDCl_3$) were referenced to the residual solvent peak. Chemical shifts (δ) are reported in parts per million (ppm) relative to residual undeuterated solvent as an internal reference. The following abbreviations were used to explain the multiplicities: s = single; d = doublet, t = triplet, q = quartet, dd = doublet of doublets, dt = doublet of triplets, m = multiplet, br = broad. Mass spectra were recorded on a JEOL spectrometer at Emory University Mass Spectrometry Center. Analytical thin layer chromatography (TLC) was performed on precoated glass backed plates from Scientific Adsorbents Incorporated (Silica Gel 60 F254; 0.25 mm thickness). Plates were visualized using ultraviolet radiation.

4.1.2. General procedure for synthesis of compounds *Ia–p*

To a solution of 1,4-bis(bromomethyl)benzene (1 mmol) in anhydrous acetonitrile (10 mL) was added potassium carbonate (3 mmol) and the corresponding secondary amine (2.2 mmol). The reaction mixture was heated at reflux for 3 h. The resulting mixture was diluted with water (20 mL) and extracted with ethyl acetate (15 mL) three times. The combined organic layers were washed with brine, dried over anhydrous sodium sulfate, and concentrated in vacuo. The crude was purified by column chromatography with methanol/dichloromethane (150:1, v/v) to give the title compound as a colorless liquid or a white solid.

*4.1.2.1. 1,4-Bis(pyrrolidin-1-ylmethyl)benzene (**Ia**).* Colorless liquid, yield 95%. ^{1}H NMR (400 MHz, $CDCl_3$) δ 7.27 (s, 4H), 3.59 (s, 4H), 2.48–2.53 (m, 8H), 1.76–1.80 (m, 8H). ^{13}C NMR (100 MHz, $CDCl_3$) δ 137.95, 128.86, 60.54, 54.21, 23.49. HRMS calcd for $C_{16}H_{25}N_2$ 245.20123 $[M+H]^+$, found 245.20084.

*4.1.2.2. 1,4-Bis(piperidin-1-ylmethyl)benzene (**Ib**).* White solid, yield 92%, m.p. 84–86 °C. ^{1}H NMR (400 MHz, $CDCl_3$) δ 7.25 (s, 4H), 3.45 (s, 4H), 2.37 (s, 8H), 1.54–1.59 (m, 8H), 1.40–1.45 (m, 4H). ^{13}C NMR (100 MHz, $CDCl_3$) δ 137.31, 129.19, 63.87, 54.70, 26.19, 24.61. HRMS calcd for $C_{18}H_{29}N_2$ 273.23253 $[M+H]^+$, found 273.23243.

*4.1.2.3. 1,4-Bis(morpholinomethyl)benzene (**Ic**).* White solid, yield 88%, m.p. 113–115 °C. ^{1}H NMR (400 MHz, $CDCl_3$) δ 7.27 (s, 4H), 3.70–3.72 (m, 8H), 3.48 (s, 4H), 2.43–2.45 (m, 8H). ^{13}C NMR (100 MHz, $CDCl_3$) δ 136.83, 129.31, 67.20, 63.38, 53.80. HRMS calcd for $C_{16}H_{25}O_2N_2$ 277.19105 $[M+H]^+$, found 277.19089.

*4.1.2.4. N,N′-(1,4-Phenylenebis(methylene))bis(N-methylaniline) (**Id**).* White solid, yield 83%, m.p. 77–79 °C. ^{1}H NMR (400 MHz, $CDCl_3$) δ 7.18–7.24 (m, 4H), 7.17 (s, 4H), 6.68–6.76 (m, 6H), 4.51 (s, 4H), 3.00 (s, 6H). ^{13}C NMR (100 MHz, $CDCl_3$) δ 149.87, 137.80, 129.32, 127.13, 116.67, 112.51, 56.51, 38.66. HRMS calcd for $C_{22}H_{25}N_2$ 317.20123 $[M+H]^+$, found 317.20070.

*4.1.2.5. N,N′-(1,4-phenylenebis(methylene))bis(4-fluoro-N-methylaniline) (**Ie**).* White solid, yield 80%, m.p. 78–80 °C. ^{1}H NMR (400 MHz, $CDCl_3$) δ 7.16 (s, 4H), 6.88–6.95 (m, 4H), 6.63–6.69 (m, 1H), 4.45 (s, 4H), 2.96 (s, 6H). ^{13}C NMR (100 MHz, $CDCl_3$) δ 156.78, 154.44, 146.65, 137.74, 127.26, 115.76, 115.54, 113.82, 113.74, 57.37, 39.23. HRMS calcd for $C_{22}H_{22}N_2F_2$ 352.17456 $[M]^+$, found 352.17423.

*4.1.2.6. N,N′-(1,4-Phenylenebis(methylene))bis(1-(2-chlorophenyl)-N-methylmethanamine) (**If**).* Colorless liquid, yield 78%. ^{1}H NMR (400 MHz, $CDCl_3$) δ 7.56 (dd, J = 1.5, 0.9 Hz, 1H), 7.54 (dd, J = 1.5, 0.9 Hz, 1H), 7.34 (d, J = 1.5 Hz, 1H), 7.32 (s, 1H), 7.32 (s, 4H), 7.22–7.26 (m, 2H), 7.14–7.19 (m, 2H), 3.63 (s, 4H), 3.57 (s, 4H), 2.20 (s, 6H). ^{13}C NMR (100 MHz, $CDCl_3$) δ 138.14, 137.14, 134.43, 130.90, 129.58, 129.01, 128.17, 126.80, 62.21, 58.67, 42.46. HRMS calcd for $C_{24}H_{27}N_2Cl_2$ 413.15458 $[M+H]^+$, found 413.15445.

*4.1.2.7. N,N′-(1,4-Phenylenebis(methylene))bis(1-(3-chlorophenyl)-N-methylmethanamine) (**Ig**).* Colorless liquid, yield 80%. ^{1}H NMR (400 MHz, $CDCl_3$) δ 7.37 (s, 2H), 7.31 (4, 1H), 7.20–7.25 (m, 6H), 3.52 (s, 4H), 3.48 (s, 4H), 2.18 (s, 6H). ^{13}C NMR (100 MHz, $CDCl_3$) δ 141.73, 137.93, 134.34, 129.67, 129.08, 127.32, 127.17, 110.22, 61.87, 61.38, 42.42. HRMS calcd for $C_{24}H_{27}N_2Cl_2$ 413.15458 $[M+H]^+$, found 413.15482.

*4.1.2.8. N,N′-(1,4-Phenylenebis(methylene))bis(1-(2-fluorophenyl)-N-methylmethanamine) (**Ih**).* Colorless liquid, yield 92%. ^{1}H NMR (400 MHz, $CDCl_3$) δ 7.44 (td, J = 7.5, 1.9 Hz, 2H), 7.31 (s, 4H), 7.19–7.25 (m, 2H), 7.11 (td, J = 7.5, 1.3 Hz, 2H), 6.99–7.04 (m, 2H), 3.59 (s, 3H), 3.54 (s, 3H), 2.20 (s, 6H). ^{13}C NMR (100 MHz, $CDCl_3$) δ 162.79, 160.35, 138.05, 131.52, 131.48, 129.01, 128.72, 128.63, 126.10, 125.95, 124.06, 124.02, 115.47, 115.24, 61.90, 54.30, 42.29. HRMS calcd for $C_{24}H_{27}N_2F_2$ 381.21368 $[M+H]^+$, found 381.21303.

*4.1.2.9. N,N′-(1,4-Phenylenebis(methylene))bis(1-(3-fluorophenyl)-N-methylmethanamine) (**Ii**).* Colorless liquid, yield 85%. ^{1}H NMR (400 MHz, $CDCl_3$) δ 7.31 (s, 4H), 7.24–7.29 (m, 2H), 7.09–7.13 (m, 4H), 6.90–6.95 (m, 2H), 3.51 (s, 4H), 3.49 (s, 4H), 2.18 (s, 6H). ^{13}C NMR (100 MHz, $CDCl_3$) δ 164.39, 161.94, 142.49, 142.42, 138.04, 129.80, 129.72, 129.00, 124.50, 124.47, 115.80, 115.59, 114.06, 113.84, 61.86, 61.43, 42.47. HRMS calcd for $C_{24}H_{27}N_2F_2$ 381.21368 $[M+H]^+$, found 381.21330.

*4.1.2.10. N,N′-(1,4-Phenylenebis(methylene))bis(1-(4-fluorophenyl)-N-methylmethanamine) (**Ij**).* White solid, yield 81%, mp 80–82 °C. ^{1}H NMR (400 MHz, $CDCl_3$) δ 7.28–7.33 (m, 8H), 6.97–7.03 (m, 4H), 3.49 (s, 4H), 3.47 (s, 4H), 2.16 (s, 6H). ^{13}C NMR (100 MHz, $CDCl_3$) δ 163.34, 160.91, 138.11, 135.27, 130.57, 130.49, 129.01, 115.28, 115.07, 61.78, 61.23, 42.37. HRMS calcd for $C_{24}H_{27}N_2F_2$ 381.21368 $[M+H]^+$,

found 381.21343.

*4.1.2.11. N,N′-(1,4-Phenylenebis(methylene))bis(1-(3-methoxyphenyl)-N-methylmethanamine) (**Ik**).* Colorless liquid, yield 87%. ^{1}H NMR (400 MHz, $CDCl_3$) δ 7.31 (s, 4H), 7.21–7.26 (m, 2H), 6.93–6.95 (m, 4H), 6.79–6.81 (m, 1H), 6.78 (dd, J = 2.7, 1.0 Hz, 1H), 3.81 (s, 6H), 3.50 (s, 4H), 3.49 (s, 4H), 2.18 (s, 6H). ^{13}C NMR (101 MHz, $CDCl_3$) δ 159.77, 141.22, 138.05, 129.30, 128.98, 121.41, 114.41, 112.56, 61.98, 61.71, 55.33, 42.49. HRMS calcd for $C_{26}H_{33}N_2O_2$ 405.25365 $[M+H]^+$, found 405.25331.

*4.1.2.12. N,N′-(1,4-Phenylenebis(methylene))bis(N-benzylethanamine) (**Il**).* Colorless liquid, yield 78%. ^{1}H NMR (400 MHz, $CDCl_3$) δ 7.36–7.39 (m, 4H), 7.29–7.33 (m, 8H), 7.20–7.24 (m, 2H), 3.57 (s, 4H), 3.55 (s, 4H), 2.50 (q, J = 7.1 Hz, 4H), 1.07 (t, J = 7.1 Hz, 6H). ^{13}C NMR (100 MHz, $CDCl_3$) δ 140.27, 138.55, 128.93, 128.73, 128.31, 126.86, 57.89, 57.65, 47.24, 12.07. HRMS calcd for $C_{26}H_{33}N_2$ 373.26383 $[M+H]^+$, found 373.26385.

*4.1.2.13. N,N′-(1,4-Phenylenebis(methylene))bis(N-benzyl-1-cyclopropylmethanamine) (**Im**).* Colorless liquid, yield 80%. ^{1}H NMR (400 MHz, $CDCl_3$) δ 7.38–7.41 (m, 4H), 7.32 (s, 4H), 7.28–7.32 (m, 4H), 7.19–7.24 (m, 2H), 3.65 (s, 4H), 3.64 (s, 4H), 2.33 (s, 2H), 2.31 (s, 2H), 0.88–0.97 (m, 2H), 0.43–0.48 (m, 4H), 0.01–0.05 (m, 4H). ^{13}C NMR (100 MHz, $CDCl_3$) δ 140.42, 138.68, 128.89, 128.68, 128.29, 126.83, 58.52, 58.37, 58.16, 8.68, 4.17. HRMS calcd for $C_{30}H_{37}N_2$ 425.29513 $[M+H]^+$, found 425.29508.

*4.1.2.14. N,N′-(1,4-Phenylenebis(methylene))bis(N-methyl-1-(pyridin-2-yl)methanamine) (**In**).* Colorless liquid, yield 82%. ^{1}H NMR (400 MHz, $CDCl_3$) δ 8.54 (dd, J = 1.8, 0.9 Hz, 1H), 8.53 (dd, J = 1.8, 1.0 Hz, 1H), 7.66 (td, J = 7.6, 1.8 Hz, 2H), 7.50–7.52 (m, 2H), 7.33 (s, 4H), 7.13–7.16 (m, 2H), 3.69 (s, 4H), 3.57 (s, 4H), 2.24 (s, 8H). ^{13}C NMR (100 MHz, $CDCl_3$) δ 159.87, 149.09, 137.83, 136.54, 128.99, 123.08, 122.02, 63.56, 61.98, 42.67. HRMS calcd for $C_{22}H_{27}N_4$ 347.22302 $[M+H]^+$, found 347.22275.

*4.1.2.15. N,N′-(1,4-Phenylenebis(methylene))bis(N-methyl-1-(pyridin-3-yl)methanamine) (**Io**).* Colorless liquid, yield 79%. ^{1}H NMR (400 MHz, $CDCl_3$) δ 8.57 (d, 2H), 8.50 (d, J = 1.7 Hz, 1H), 8.49 (d, J = 1.7 Hz, 1H), 7.71–7.72 (m, 1H), 7.69–7.70 (m, 1H), 7.31 (s, 4H), 7.24–7.28 (m, 2H), 3.53 (s, 4H), 3.52 (s, 4H), 2.19 (s, 6H). ^{13}C NMR (100 MHz, $CDCl_3$) δ 150.42, 148.63, 137.90, 136.78, 134.88, 129.04, 123.55, 61.82, 59.06, 42.40. HRMS calcd for $C_{22}H_{27}N_4$ 347.22302 $[M+H]^+$, found 347.22288.

*4.1.2.16. N,N′-(1,4-Phenylenebis(methylene))bis(N-methyl-1-(pyridin-4-yl)methanamine) (**Ip**).* Colorless liquid, yield 80%. ^{1}H NMR (400 MHz, $CDCl_3$) δ 8.54–8.55 (m, 4H), 7.31–7.33 (m, 8H), 3.53 (s, 4H), 3.51 (s, 4H), 2.20 (s, 6H). ^{13}C NMR (100 MHz, $CDCl_3$) δ 149.80, 149.02, 137.87, 129.01, 123.94, 61.96, 60.72, 42.61. HRMS calcd for $C_{22}H_{27}N_4$ 347.22302 $[M+H]^+$, found 347.22290.

*4.1.3. General procedure for synthesis of compounds **IIa–p***

To a solution of 2,6-bis(chloromethyl)pyridine (1 mmol) in anhydrous acetonitrile (10 mL) was added cesium carbonate (3 mmol) and the corresponding secondary amine (2.2 mmol). The reaction mixture was heated at reflux for 5 h. The resulting mixture was diluted with water (20 mL) and extracted with ethyl acetate (15 mL) three times. The combined organic layers were washed with brine, dried over anhydrous sodium sulfate, and concentrated in vacuo. The crude was purified by column chromatography with methanol/dichloromethane (100:1, v/v) to give the title compound as a colorless liquid or a white solid.

*4.1.3.1. 2,6-Bis(pyrrolidin-1-ylmethyl)pyridine (**IIa**).* Colorless liquid, yield 86%. ^{1}H NMR (400 MHz, $CDCl_3$) δ 7.58 (t, J = 7.7 Hz, 1H), 7.25 (s, 1H), 7.24 (s, 1H), 3.75 (s, 4H), 2.52–2.58 (m, 8H), 1.73–1.81 (m, 8H). ^{13}C NMR (100 MHz, $CDCl_3$) δ 158.77, 136.89, 121.15, 62.41, 54.43, 23.69. HRMS calcd for $C_{15}H_{24}N_3$ 246.19647 $[M+H]^+$, found 246.19644.

*4.1.3.2. 2,6-Bis(piperidin-1-ylmethyl)pyridine (**IIb**).* Colorless liquid, yield 80%. ^{1}H NMR (400 MHz, $CDCl_3$) δ 7.59 (t, J = 7.7 Hz, 1H), 7.29 (s, 1H), 7.27 (s, 1H), 3.60 (s, 4H), 2.42–2.44 (m, 8H), 1.55–1.61 (m, 8H), 1.40–1.46 (m, 4H). ^{13}C NMR (100 MHz, $CDCl_3$) δ 158.71, 136.67, 121.20, 65.57, 54.99, 26.20, 24.52. HRMS calcd for $C_{17}H_{28}N_3$ 274.22777 $[M+H]^+$, found 274.22757.

*4.1.3.3. 2,6-Bis(morpholinomethyl)pyridine (**IIc**).* White solid, yield 90%, m.p. 93–95 °C. ^{1}H NMR (400 MHz, $CDCl_3$) δ 7.63 (t, J = 7.7 Hz, 1H), 7.32 (s, 1H), 7.31 (s, 1H), 3.73 (t, 8H), 3.66 (s, 4H), 2.51 (t, 8H). ^{13}C NMR (100 MHz, $CDCl_3$) δ 157.90, 136.86, 121.56, 67.14, 65.02, 53.92. HRMS calcd for $C_{15}H_{24}O_2N_3$ 278.18630 $[M+H]^+$, found 278.18562.

*4.1.3.4. N,N′-(Pyridine-2,6-diylbis(methylene))bis(N-methylaniline) (**IId**).* White solid, yield 75%, m.p. 91–93 °C. ^{1}H NMR (400 MHz, $CDCl_3$) δ 7.49 (t, J = 7.7 Hz, 1H), 7.20–7.25 (m, 4H), 7.02 (s, 1H), 7.00 (s, 1H), 6.70–6.75 (m, 6H), 4.65 (s, 4H), 3.13 (s, 6H). ^{13}C NMR (100 MHz, $CDCl_3$) δ 159.44, 149.41, 137.61, 129.41, 119.01, 116.82, 112.32, 59.00, 39.24. HRMS calcd for $C_{21}H_{24}N_3$ 318.19647 $[M+H]^+$, found 318.19664.

*4.1.3.5. N,N′-(Pyridine-2,6-diylbis(methylene))bis(4-fluoro-N-methylaniline) (**IIe**).* Colorless liquid, yield 70%. ^{1}H NMR (400 MHz, $CDCl_3$) δ 7.52 (t, J = 7.7 Hz, 1H), 7.03 (t, J = 0.8 Hz, 1H), 7.01 (t, J = 0.8 Hz, 1H), 6.90–6.95 (m, 4H), 6.63–6.66 (m, 4H), 4.59 (s, 4H), 3.08 (s, 6H). ^{13}C NMR (101 MHz, $CDCl_3$) δ 159.34, 156.83, 154.49, 146.14, 137.64, 129.87, 128.55, 119.19, 115.86, 115.64, 113.45, 113.38, 59.63, 39.85. HRMS calcd for $C_{21}H_{22}F_2N_3$ 354.17763 $[M+H]^+$, found 354.17776.

*4.1.3.6. N,N′-(Pyridine-2,6-diylbis(methylene))bis(1-(2-chlorophenyl)-N-methylmethanamine) (**IIf**).* Colorless liquid, yield 80%. ^{1}H NMR (400 MHz, $CDCl_3$) δ 7.63 (t, J = 7.7 Hz, 1H), 7.57 (d, J = 1.8 Hz, 1H), 7.55 (d, J = 1.8 Hz, 1H), 7.42 (s, 1H), 7.40 (s, 1H), 7.34 (d, J = 1.5 Hz, 1H), 7.33 (d, J = 1.5 Hz, 1H), 7.15–7.25 (m, 4H), 3.77 (s, 4H), 3.72 (s, 4H), 2.29 (s, 6H). ^{13}C NMR (100 MHz, $CDCl_3$) δ 158.88, 137.10, 136.75, 134.51, 130.97, 129.63, 128.32, 126.79, 121.33, 63.86, 58.85, 42.77. HRMS calcd for $C_{23}H_{26}N_3Cl_2$ 414.14983 $[M+H]^+$, found 414.14968.

*4.1.3.7. N,N′-(Pyridine-2,6-diylbis(methylene))bis(1-(3-chlorophenyl)-N-methylmethanamine) (**IIg**).* Colorless liquid, yield 77%. ^{1}H NMR (399 MHz, $CDCl_3$) δ 7.68 (t, J = 7.7 Hz, 1H), 7.39–7.41 (m, 4H), 7.20–7.25 (m, 6H), 3.70 (s, 4H), 3.55 (s, 4H), 2.24 (s, 6H). ^{13}C NMR (100 MHz, $CDCl_3$) δ 158.91, 141.55, 137.11, 134.34, 129.65, 129.08, 127.34, 127.16, 121.27, 63.69, 61.60, 42.76. HRMS calcd for $C_{23}H_{26}N_2Cl_2$ 414.14983 $[M+H]^+$, found 414.14902.

*4.1.3.8. N,N′-(Pyridine-2,6-diylbis(methylene))bis(1-(2-fluorophenyl)-N-methylmethanamine) (**IIh**).* Colorless liquid, yield 79%. ^{1}H NMR (400 MHz, $CDCl_3$) δ 7.65 (t, J = 7.7 Hz, 1H), 7.45 (td, J = 7.5, 1.9 Hz, 2H), 7.41 (s, 1H), 7.39 (s, 1H), 7.20–7.25 (m, 2H), 7.10 (td, J = 7.5, 1.3 Hz, 2H), 6.99–7.04 (m, 2H), 3.73 (s, 4H), 3.66 (s, 4H), 2.26 (s, 6H). ^{13}C NMR (100 MHz, $CDCl_3$) δ 162.76, 160.31, 158.86, 136.98, 131.57, 131.53, 128.81, 128.73, 125.67, 125.52, 123.98, 123.94, 121.21, 115.46, 115.24, 63.59, 54.60, 54.58, 42.47. HRMS calcd for $C_{23}H_{26}N_3F_2$ 382.20893 $[M+H]^+$, found 382.20767.

*4.1.3.9. N,N′-(Pyridine-2,6-diylbis(methylene))bis(1-(3-fluorophenyl)-N-methylmethanamine) (**IIi**).* Colorless liquid, yield 80%. ^{1}H NMR (400 MHz, $CDCl_3$) δ 7.68 (t, J = 7.7 Hz, 1H), 7.42 (s, 1H), 7.40 (s, 1H), 7.23–7.29 (m, 2H), 7.13–7.15 (m, 2H), 7.11–7.12 (m, 2H), 6.90–6.95 (m, 2H), 3.70 (s, 4H), 3.57 (s, 4H), 2.25 (s, 6H). ^{13}C NMR (100 MHz, $CDCl_3$) δ 164.31, 161.87, 158.89, 142.10, 142.03, 137.07, 129.77, 129.69, 124.49, 124.47, 121.17, 115.78, 115.56, 114.08, 113.87, 63.58, 61.59, 61.58, 42.68. HRMS calcd for $C_{23}H_{26}N_3F_2$ 382.20893 $[M+H]^+$, found 382.20915.

*4.1.3.10. N,N′-(Pyridine-2,6-diylbis(methylene))bis(1-(4-fluorophenyl)-N-methylmethanamine) (**IIj**).* Colorless liquid, yield 77%. ^{1}H NMR (400 MHz, $CDCl_3$) δ 7.66 (t, J = 7.7 Hz, 1H), 7.39 (s, 1H), 7.37 (s, 1H), 7.30–7.35 (m, 4H), 6.96–7.02 (m, 4H), 3.68 (s, 4H), 3.54 (s, 4H), 2.22 (s, 6H). ^{13}C NMR (100 MHz, $CDCl_3$) δ 163.28, 160.84, 158.94, 136.96, 134.86, 134.83, 130.55, 130.47, 121.14, 115.21, 115.00, 63.44, 61.34, 42.54. HRMS calcd for $C_{23}H_{26}N_3F_2$ 382.20893 $[M+H]^+$, found 382.20773.

*4.1.3.11. N,N′-(Pyridine-2,6-diylbis(methylene))bis(1-(3-methoxyphenyl)-N-methylmethanamine) (**IIk**).* Colorless liquid, yield 90%. ^{1}H NMR (400 MHz, $CDCl_3$) δ 7.65 (dd, J = 7.9, 7.4 Hz, 1H), 7.42 (s, 1H), 7.40 (s, 1H), 7.20–7.24 (m, 2H), 6.94–6.97 (m, 4H), 6.80 (dd, J = 2.7, 1.4 Hz, 1H), 6.78 (dd, J = 2.7, 1.4 Hz, 1H), 3.81 (s, 6H), 3.69 (s, 4H), 3.56 (s, 4H), 2.25 (s, 6H). ^{13}C NMR (100 MHz, $CDCl_3$) δ 159.79, 159.13, 141.01, 137.03, 129.35, 121.45, 121.14, 114.49, 112.61, 63.63, 62.24, 55.38, 42.81. HRMS calcd for $C_{25}H_{32}N_3O_2$ 406.24890 $[M+H]^+$, found 406.24852.

*4.1.3.12. N,N′-(Pyridine-2,6-diylbis(methylene))bis(N-benzylethanamine) (**IIl**).* Colorless liquid, yield 86%. ^{1}H NMR (400 MHz, $CDCl_3$) δ 7.62 (t, J = 7.7 Hz, 1H), 7.44 (s, 1H), 7.42 (s, 1H), 7.36–7.39 (m, 4H), 7.26–7.32 (m, 4H), 7.19–7.23 (m, 2H), 3.72 (s, 4H), 3.62 (s, 4H), 2.55 (q, J = 7.1 Hz, 4H), 1.08 (t, J = 7.1 Hz, 6H). ^{13}C NMR (100 MHz, $CDCl_3$) δ 159.75, 139.86, 136.84, 128.88, 128.28, 126.89, 120.61, 59.87, 58.16, 47.80, 12.15. HRMS calcd for $C_{25}H_{32}N_3$ 374.25907 $[M+H]^+$, found 374.25907.

*4.1.3.13. N,N′-(Pyridine-2,6-diylbis(methylene))bis(N-benzyl-1-cyclopropylmethanamine) (**IIm**).* Colorless liquid, yield 72%. ^{1}H NMR (400 MHz, $CDCl_3$) δ 7.64 (dd, J = 8.1, 7.2 Hz, 1H), 7.50 (s, 1H), 7.48 (s, 1H), 7.40–7.42 (m, 4H), 7.28–7.33 (m, 4H), 7.20–7.24 (m, 2H), 3.84 (s, 4H), 3.71 (s, 4H), 2.40 (s, 2H), 2.38 (s, 2H), 0.89–0.99 (m, 2H), 0.43–0.48 (m, 4H), 0.01–0.07 (m, 4H). ^{13}C NMR (100 MHz, $CDCl_3$) δ 159.88, 140.08, 136.85, 128.88, 128.33, 126.92, 120.66, 60.34, 59.01, 58.71, 8.72, 4.15. HRMS calcd for $C_{29}H_{36}N_3$ 426.29037 $[M+H]^+$, found 426.28990.

*4.1.3.14. N,N′-(Pyridine-2,6-diylbis(methylene))bis(N-methyl-1-(pyridin-2-yl)methanamine) (**IIn**).* Colorless liquid, yield 75%. ^{1}H NMR (400 MHz, $CDCl_3$) δ 8.51 (dd, J = 1.8, 0.9 Hz, 1H), 8.50 (dd, J = 1.8, 0.9 Hz, 1H), 7.64 (d, J = 1.7 Hz, 1H), 7.62 (d, J = 1.7 Hz, 1H), 7.60 (d, J = 1.7 Hz, 1H), 7.49 (t, J = 7.8, 1.1 Hz, 1H), 7.47 (t, J = 7.8, 1.1 Hz, 1H), 7.38 (s, 1H), 7.36 (s, 1H), 7.13 (dd, J = 4.9, 1.2 Hz, 1H), 7.11 (dd, J = 4.9, 1.2 Hz, 1H), 3.74 (s, 4H), 3.73 (s, 4H), 2.27 (s, 6H). ^{13}C NMR (100 MHz, $CDCl_3$) δ 159.31, 158.63, 149.17, 137.03, 136.60, 123.23, 122.15, 121.41, 63.70, 63.63, 42.83. HRMS calcd for $C_{21}H_{26}N_5$ 348.21827 $[M+H]^+$, found 348.21800.

*4.1.3.15. N,N′-(Pyridine-2,6-diylbis(methylene))bis(N-methyl-1-(pyridin-3-yl)methanamine) (**IIo**).* Colorless liquid, yield 74%. ^{1}H NMR (400 MHz, $CDCl_3$) δ 8.59 (d, J = 0.8 Hz, 1H), 8.59 (d, J = 0.8 Hz, 1H), 8.50 (d, J = 1.7 Hz, 1H), 8.49 (d, J = 1.7 Hz, 1H), 7.72 (t, J = 2.0 Hz, 1H), 7.70 (t, J = 2.0 Hz, 1H), 7.67 (t, J = 7.7 Hz, 1H), 7.40 (s, 1H), 7.38 (s, 1H), 7.28–7.23 (m, 2H), 3.71 (s, 4H), 3.59 (s, 4H), 2.25 (s, 6H). ^{13}C NMR (100 MHz, $CDCl_3$) δ 158.80, 150.56, 148.73, 137.16, 136.75, 134.61, 123.48, 121.34, 63.60, 59.38, 42.70. HRMS calcd for $C_{21}H_{26}N_5$ 348.21827 $[M+H]^+$, found 348.21814.

*4.1.3.16. N,N′-(Pyridine-2,6-diylbis(methylene))bis(N-methyl-1-(pyridin-4-yl)methanamine) (**IIp**).* Colorless liquid, yield 81%. ^{1}H NMR (400 MHz, $CDCl_3$) δ 8.53–8.55 (m, 4H), 7.69 (t, J = 7.7 Hz, 1H), 7.42 (s, 1H), 7.40 (s, 1H), 7.32–7.34 (m, 4H), 3.71 (s, 4H), 3.59 (s, 4H), 2.27 (s, 6H). ^{13}C NMR (100 MHz, $CDCl_3$) δ 158.70, 149.88, 148.62, 137.25, 123.92, 121.35, 63.72, 60.97, 42.91. HRMS calcd for $C_{21}H_{26}N_5$ 348.21827 $[M+H]^+$, found 348.21813.

4.2. Primary binding affinity screening

For binding affinity assay, 2×10^4 MDA-MB-231 cells in 300 μL of cell culture medium were seeded in an 8-well slide chamber 2 days before the experiments were conducted. Various concentrations of different compounds (1, 10, 100, or 1000 nM) were added to the separate wells and incubated for 10 min at room temperature, and then the cells were fixed in 4% ice-cold paraformaldehyde. The cells were rehydrated in phosphate-buffered saline (PBS). The slides were subsequently incubated for 30 min at room temperature with 0.05 μg/mL biotinylated **TN14003**, washed three times with PBS, and incubated in streptavidin-rhodamine (1:150 dilution; Jackson ImmunoResearch Laboratories, West Grove, PA) for 30 min at room temperature. Finally, the slides were washed with PBS and mounted in an anti-fade mounting solution (Molecular Probes, Eugene, OR), and the samples were analyzed on a Nikon Eclipse E800 microscope [31,34].

4.3. Matrigel invasion assay

Matrigel invasion assay was performed by using a Matrigel invasion chamber from Corning Biocoat (Bedford MA). CXCL12α (200 ng/mL; R & D Systems, Minneapolis, MN) was added to the bottom chamber to induce the invasion of MDA-MB-231 cells through the Matrigel. The selected compounds or AMD3100 were added to the cells (100 nM) before the cells were seeded in the top chamber. The Matrigel invasion chamber was incubated for 22 h in a humidified cell culture incubator. First, non-invading cells were removed from the top of the Matrigel with a cotton-tipped swab. Invading cells on the filter at the bottom of the Matrigel were fixed in methanol and stained with hematoxylin and eosin (H&E). The percent of invasion was determined by counting the H&E stained cells [31,34].

4.4. Paw inflammation suppression test

Acute inflammation was induced by subcutaneous injection of 50 μL of λ-carrageenan (1% w/v in saline) into one of the hind paws of the female C57BL/6J mice (Jackson Laboratories); the other hind paw was injected with 50 μL of saline, which was used as a non-inflammation control. The selected compounds were dissolved in 10% DMSO and 90% of 45% (2-hydroxypropyl)-β-cyclodextrin (CD) in PBS. In the treatment group, compounds **IIg**, **IIk**, **IIm** and **IIn** were administered intraperitoneally (i.p.) at 10 mg/kg daily, while TN14003 was administered at 300 μg/kg, i.p., daily, 30 min following carrageenan challenge. The rationale for using 300 μg/kg for TN14003 was that we found this concentration to be the minimum concentration needed to achieve the maximum efficacy of this compound in a breast cancer metastasis animal model [41]. Control animals received corresponding i.p. injections of the vehicle. The animals were sacrificed 74 h after carrageenan challenge and 2 h after the last injection of the selected compounds. The final paws were photographed and measured for thickness from

the “palm” to the back of the paw with a caliper. These were compared to the volume of carrageenan-untreated contralateral paw to obtain the edema volume; the volume of the contralateral paw was subtracted from the volume of the carrageenan injected paw to obtain the edema volume. The inflammation-suppression percentage was calculated by comparing the drug-treated group to the control group. Five mice per group were used to determine the effect of the CXCR4 inhibitors as previously described [27,31].

4.5. Molecular modeling (docking) studies

The docking experiment was performed by Schrodinger Maestro Package [42]. The crystal structure of CXCR4 (PDB code: 3ODU [40]) was processed following the established Protein Prepare Wizard workflow to obtain the receptor structure suitable for docking [43]. All water molecules were deleted and only Chain A was used to prepare the receptor. All residues beyond 20 Å of the ligand were removed to accelerate the calculation speed. The binding site was selected using the default Receptor Grid Generation procedure and the docking grid was generated around the co-crystalized small molecule ligand IT1t. The **IIn** ligand was initially drawn by ChemDraw as a 2D structure and then prepared by the Ligprep application to obtain the 3D conformers for docking [44]. The prepared ligand was then flexibly docked onto the receptor using Glide [45] and the default setting parameters with no constrains. 10 docking poses were obtained and the one with the best Glide score was chosen to study the interaction. The plot (Fig. 8) was constructed using Pymol version 0.99 [46].

Acknowledgments

This study was financially supported by a research grant from NIH NCI (R01 CA165306). We thank Ms. Jessica Paulishen and Mr. Andrew Teodorescu for proof-reading.

Appendix A. Supplementary data

Supplementary data related to this article can be found at http://dx.doi.org/10.1016/j.ejmech.2016.04.040.

References

[1] B. Debnath, S. Xu, F. Grande, A. Garofalo, N. Neamati, Small molecule inhibitors of CXCR4, Theranostics 3 (2013) 47–75.
[2] D. Das, K. Maeda, Y. Hayashi, N. Gavande, D.V. Desai, S.B. Chang, A.K. Ghosh, H. Mitsuya, Insights into the mechanism of inhibition of CXCR4: identification of Piperidinylethanamine analogs as anti-HIV-1 inhibitors, Antimicrob. Agents Chemother. 59 (2015) 1895–1904.
[3] S. Poty, P. Desogere, C. Goze, F. Boschetti, T. D'Huys, D. Schols, C. Cawthorne, S.J. Archibald, H.R. Maecke, F. Denat, New AMD3100 derivatives for CXCR4 chemokine receptor targeted molecular imaging studies: synthesis, anti-HIV-1 evaluation and binding affinities, Dalton. Trans. 44 (2015) 5004–5016.
[4] M.C. Blades, A. Manzo, F. Ingegnoli, P.R. Taylor, G.S. Panayi, H. Irjala, S. Jalkanen, D.O. Haskard, M. Perretti, C. Pitzalis, Stromal cell-derived factor 1 (CXCL12) induces human cell migration into human lymph nodes transplanted into SCID mice, J. Immunol. 168 (2002) 4308–4317.
[5] Y.X. Liao, Z.Z. Fu, C.H. Zhou, L.C. Shan, Z.Y. Wang, F. Yin, L.P. Zheng, Y.Q. Hua, Z.D. Cai, AMD3100 reduces CXCR4-mediated survival and metastasis of osteosarcoma by inhibiting JNK and Akt, but not p38 or Erk1/2, pathways in *in vitro* and mouse experiments, Oncol. Rep. 34 (2015) 33–42.
[6] Z.G. Zachariassen, S. Thiele, E.A. Berg, P. Rasmussen, T. Fossen, M.M. Rosenkilde, J. Våbenø, B.E. Haug, Design, synthesis, and biological evaluation of scaffold-based tripeptidomimetic antagonists for CXC chemokine receptor 4 (CXCR4), Bioorg. Med. Chem. 22 (2014) 4759–4769.
[7] Y. Kang, P.M. Siegel, W. Shu, M. Drobnjak, S.M. Kakonen, C. Cordon-Cardo, T.A. Guise, J. Massague, A multigenic program mediating breast cancer metastasis to bone, Cancer Cell 3 (2003) 537–549.
[8] A. Muller, B. Homey, H. Soto, N. Ge, D. Catron, M.E. Buchanan, T. McClanahan, E. Murphy, W. Yuan, S.N. Wagner, J.L. Barrera, A. Mohar, E. Verastegui, A. Zlotnik, Involvement of chemokine receptors in breast cancer metastasis, Nature 410 (2001) 50–56.
[9] M. Burger, T. Hartmann, M. Krome, J. Rawluk, H. Tamamura, N. Fujii, T.J. Kipps, J.A. Burger, Small peptide inhibitors of the CXCR4 chemokine receptor (CD184) antagonize the activation, migration, and antiapoptotic responses of CXCL12 in chronic lymphocytic leukemia B cells, Blood 106 (2005) 1824–1830.
[10] L.E. Woodard, S. Nimmagadda, CXCR4-based imaging agents, J. Nucl. Med. 52 (2011) 1665–1669.
[11] F. Balkwill, Cancer and the chemokine network, Nat. Rev. Cancer 4 (2004) 540–550.
[12] Y.M. Li, Y. Pan, Y. Wei, X. Cheng, B.P. Zhou, M. Tan, X. Zhou, W. Xia, G.N. Hortobagyi, D. Yu, M.C. Hung, Upregulation of CXCR4 is essential for HER2-mediated tumor metastasis, Cancer Cell 6 (2004) 459–469.
[13] O. Salvucci, A. Bouchard, A. Baccarelli, J. Deschenes, G. Sauter, R. Simon, R. Bianchi, M. Basik, The role of CXCR4 receptor expression in breast cancer: a large tissue microarray study, Breast Cancer Res. Treat. 97 (2006) 275–283.
[14] M. Allegretti, M.C. Cesta, A. Garin, A.E. Proudfoot, Current status of chemokine receptor inhibitors in development, Immunol. Lett. 145 (2012) 68–78.
[15] M. Burger, A. Glodek, T. Hartmann, A. Schmitt-Graff, L.E. Silberstein, N. Fujii, T.J. Kipps, J.A. Burger, Functional expression of CXCR4 (CD184) on small-cell lung cancer cells mediates migration, integrin activation, and adhesion to stromal cells, Oncogene 22 (2003) 8093–8101.
[16] J. Wang, J. Wang, Y. Sun, W. Song, J.E. Nor, C.Y. Wang, R.S. Taichman, Diverse signaling pathways through the CXCL12/CXCR4 chemokine axis in prostate cancer cell lines leads to altered patterns of cytokine secretion and angiogenesis, Cell. Signal. 17 (2005) 1578–1592.
[17] T. El Rayes, R. Catena, S. Lee, M. Stawowczyk, N. Joshi, C. Fischbach, C.A. Powell, A.J. Dannenberg, N.K. Altorki, D. Gao, V. Mittal, Lung inflammation promotes metastasis through neutrophil protease-mediated degradation of Tsp-1, Proc. Natl. Acad. Sci. U. S. A. 112 (2015) 16000–16005.
[18] B. Jiang, X. Huang, H. Yao, J. Jiang, X. Wu, S. Jiang, Q. Wang, T. Lu, J. Xu, Discovery of potential anti-inflammatory drugs: diaryl-1,2,4-triazoles bearing N-hydroxyurea moiety as dual inhibitors of cyclooxygenase-2 and 5-lipoxygenase, Org. Biomol. Chem. 12 (2014) 2114–2127.
[19] E. Rahme, S. Bernatsky, NSAIDs and risk of lower gastrointestinal bleeding, Lancet 376 (2010) 146–148.
[20] E.Z. Dajani, K. Islam, Cardiovascular and gastrointestinal toxicity of selective cyclo-oxygenase-2 inhibitors in man, J. Physiol. Pharmacol. 59 (2008) 117–133.
[21] E. Fosslien, Adverse effects of nonsteroidal anti-inflammatory drugs on the gastrointestinal system, Ann. Clin. Lab. Sci. 28 (1998) 67–81.
[22] D.H. Solomon, Selective cyclooxygenase 2 inhibitors and cardiovascular events, Arthritis Rheum. 52 (2005) 1968–1978.
[23] J.M. Dogne, C.T. Supuran, D. Pratico, Adverse cardiovascular effects of the coxibs, J. Med. Chem. 48 (2005) 2251–2257.
[24] S. Hummel, H. Van Aken, A. Zarbock, Inhibitors of CXC chemokine receptor type 4: putative therapeutic approaches in inflammatory diseases, Curr. Opin. Hematol. 21 (2014) 29–36.
[25] W.T. Choi, S. Duggineni, Y. Xu, Z. Huang, J. An, Drug discovery research targeting the CXC chemokine receptor 4 (CXCR4), J. Med. Chem. 55 (2012) 977–994.
[26] E. De Clercq, The bicyclam AMD3100 story, Nat. Rev. Drug Discov. 2 (2003) 581–587.
[27] Z. Liang, W. Zhan, A. Zhu, Y. Yoon, S. Lin, M. Sasaki, J.M. Klapproth, H. Yang, H.E. Grossniklaus, J. Xu, M. Rojas, R.J. Voll, M.M. Goodman, R.F. Arrendale, J. Liu, C.C. Yun, J.P. Snyder, D.C. Liotta, H. Shim, Development of a unique small molecule modulator of CXCR4, PloS One 7 (2012) e34038.
[28] M.K. Schwarz, T.N. Wells, New therapeutics that modulate chemokine networks, Nat. Rev. Drug Discov. 1 (2002) 347–358.
[29] A. Scozzafava, A. Mastrolorenzo, C.T. Supuran, Non-peptidic chemokine receptors antagonists as emerging anti-HIV agents, J. Enzyme Inhib. Med. Chem. 17 (2002) 69–76.
[30] W. Zhan, Z. Liang, A. Zhu, S. Kurtkaya, H. Shim, J.P. Snyder, D.C. Liotta, Discovery of small molecule CXCR4 antagonists, J. Med. Chem. 50 (2007) 5655–5664.
[31] A. Zhu, W. Zhan, Z. Liang, Y. Yoon, H. Yang, H.E. Grossniklaus, J. Xu, M. Rojas, M. Lockwood, J.P. Snyder, D.C. Liotta, H. Shim, Dipyrimidine amines: a novel class of chemokine receptor type 4 antagonists with high specificity, J. Med. Chem. 53 (2010) 8556–8568.
[32] S.R. Mooring, T. Gaines, Z. Liang, H. Shim, Synthesis of pyridine derivatives as potential antagonists of chemokine receptor type 4, Heterocycl. Comm. 20 (2014) 149–153.
[33] Y. Wang, S.T. Hazeldine, J. Li, D. Oupicky, Development of functional poly(-amido amine) CXCR4 antagonists with the ability to mobilize leukocytes and deliver nucleic acids, Adv. Healthc. Mater 4 (2015) 729–738.
[34] S.R. Mooring, J. Liu, Z. Liang, J. Ahn, S. Hong, Y. Yoon, J.P. Snyder, H. Shim, Benzenesulfonamides: a unique class of chemokine receptor type 4 inhibitors, ChemMedChem 8 (2013) 622–632.
[35] H.K. Shu, Y. Yoon, S. Hong, K. Xu, H. Gao, C. Hao, E. Torres-Gonzalez, C. Nayra, M. Rojas, H. Shim, Inhibition of the CXCL12/CXCR4-axis as preventive therapy for radiation-induced pulmonary fibrosis, PloS One 8 (2013) e79768.
[36] K. Fosgerau, T. Hoffmann, Peptide therapeutics: current status and future directions, Drug Discov. Today 20 (2015) 122–128.
[37] R. Vinegar, J.F. Truax, J.L. Selph, P.R. Johnston, A.L. Venable, K.K. McKenzie, Pathway to carrageenan-induced inflammation in the hind limb of the rat, Fed. Proc. 46 (1987) 118–126.
[38] T. Lawrence, The nuclear factor NF-kappaB pathway in inflammation, Cold

Spring Harb. Perspect. Biol. 1 (2009) a001651.
[39] Y.J. Wan, M.Z. Badr, Inhibition of carrageenan-induced cutaneous inflammation by PPAR agonists is dependent on hepatocyte-specific retinoid X ReceptorAlpha, PPAR Res. 2006 (2006) 96341.
[40] B. Wu, E.Y. Chien, C.D. Mol, G. Fenalti, W. Liu, V. Katritch, R. Abagyan, A. Brooun, P. Wells, F.C. Bi, D.J. Hamel, P. Kuhn, T.M. Handel, V. Cherezov, R.C. Stevens, Structures of the CXCR4 chemokine GPCR with small-molecule and cyclic peptide antagonists, Science 330 (2010) 1066–1071.
[41] Y. Yoon, Z. Liang, X. Zhang, M. Choe, A. Zhu, H.T. Cho, D.M. Shin, M.M. Goodman, Z.G. Chen, H. Shim, CXC chemokine receptor-4 antagonist blocks both growth of primary tumor and metastasis of head and neck cancer in xenograft mouse models, Cancer Res. 67 (2007) 7518–7524.
[42] Schrödinger Release 2015-4: Maestro, Version 10.4, Schrödinger, LLC, New York, NY, 2015.
[43] Protein Preparation Wizard, Schrödinger, LLC, New York, NY, 2012.
[44] Ligprep, Version 3.6, Schrödinger, LLC, New York, NY, 2015.
[45] Glide, Version 6.9, Schrödinger, LLC, New York, NY, 2015.
[46] Glide, version 0.99, Schrödinger, LLC, New York, NY.